



**HAL**  
open science

## Evidence of strain induced structural change in hetero-epitaxial NdNiO<sub>3</sub> thin films with metal-insulator transition

P. Laffez, O I Lebedev, P. Ruello, R. Desfeux, G. Banerjee, Fabien Capon

### ► To cite this version:

P. Laffez, O I Lebedev, P. Ruello, R. Desfeux, G. Banerjee, et al.. Evidence of strain induced structural change in hetero-epitaxial NdNiO<sub>3</sub> thin films with metal-insulator transition. *European Physical Journal: Applied Physics*, 2004, 25 (1), pp.25-31. 10.1051/epjap:2003087 . hal-03935795

**HAL Id: hal-03935795**

**<https://hal.science/hal-03935795>**

Submitted on 12 Jan 2023

**HAL** is a multi-disciplinary open access archive for the deposit and dissemination of scientific research documents, whether they are published or not. The documents may come from teaching and research institutions in France or abroad, or from public or private research centers.

L'archive ouverte pluridisciplinaire **HAL**, est destinée au dépôt et à la diffusion de documents scientifiques de niveau recherche, publiés ou non, émanant des établissements d'enseignement et de recherche français ou étrangers, des laboratoires publics ou privés.

# Evidence of strain induced structural change in hetero-epitaxial NdNiO<sub>3</sub> thin films with metal-insulator transition

P. Laffez<sup>1,a</sup>, O.I. Lebedev<sup>2</sup>, P. Ruello<sup>1</sup>, R. Desfeux<sup>3</sup>, G. Banerjee<sup>4</sup>, and F. Capon<sup>1</sup>

<sup>1</sup> Laboratoire de Physique de l'État Condensé, UMR CNRS 6087, Université du Maine, avenue O. Messiaen, 72085 Le Mans Cedex, France

<sup>2</sup> EMAT, University of Antwerp, Groenenborgerlaan 171, 2020 Antwerp, Belgium

<sup>3</sup> Laboratoire de Physico-Chimie des Interfaces et Applications, Université d'Artois, rue Jean Souvraz, SP 18, 62307 Lens Cedex, France

<sup>4</sup> Exp. Cond. Matter Physics Division, Saha Institute of Nuclear Physics 1/AF Bidhan Nagar, Calcutta 700064, India

**Abstract.** Neodymium nickelate thin films have been prepared on NdGaO<sub>3</sub> substrates by RF magnetron sputtering and post-annealing treatment under oxygen pressure. Transport properties are found to depend strongly on film thickness. Thick films show transport properties close to bulk ceramics, while very thin films exhibit a large transition from metal to insulator which occurs over a wide temperature range with high resistivity. Structure and surface morphology of the films have been investigated by Transmission Electron Microscopy (TEM) and Atomic Force Microscopy (AFM). Thin films ( $\approx 17$  nm) grow heteroepi-taxially, while thicker films ( $\approx 73$  nm) show a granular structure. The thinnest sample suggests a symmetry change induced by the epitaxial strain of the substrate. This paper discusses the relationship between microstructure and transport properties.

**PACS.** 73.50.-h Electronic transport phenomena in thin films – 71.30.+h Metal-insulator transitions and other electronic transitions – 73.61.-r Electrical properties of specific thin films

## 1 Introduction

Due to its metal-insulator transition [1] and thermochromic properties [2,3] the rare-earth nickelate perovskite NdNiO<sub>3</sub> has received a great deal of attention for the last ten years. The metal-insulator transition has been correlated to the closing of the Ni-O-Ni angle which decreases the O<sub>2p</sub>-Ni<sub>3d</sub> overlap, and, hence increases the charge-transfer gap  $E_g$  [4,5]. More recently, Raman and electron diffraction studies have shown that a slight monoclinic structural phase distortion also occurs at  $T_{MI}$ , simultaneously with the electronic transition [6].

Such unusual electronic and optical features are all the more interesting since the  $T_{MI}$  can be tuned by changing the rare earth cation  $R$  [1,3,7], or by applying high pressure [8]. Research has shown that high isostatic pressure (3–15 kbar) stabilizes the metallic phase by closing the charge transfer gap  $E_g$  and decreasing the value of  $T_{MI}$ . The case of thin films grown on a substrate with lattice mismatch ( $\Delta a$ ) usually involves very high strain at the substrate-film interface. For example, in the case of an as-deposited NdNiO<sub>3</sub> film on (110) oriented single crystalline NdGaO<sub>3</sub>, the interfacial stress can be estimated to be  $G \times (\Delta a/a) \sim 6$  kbar, which is rather considerable.

Changes in crystallographic structure symmetry or strong crystallographic distortions may occur depending on both the correlation length of the interfacial strain field and the film thickness. This effect can either extend within the entire film, or relax through the film.

In order to address this issue, we have prepared several NdNiO<sub>3</sub> films of different thickness and measured both their structural and transport properties. We study the correlation of the structure, microstructure, and the electronic transport of NdNiO<sub>3</sub>. Our goal is to demonstrate that the substrate can induce such a high strain that the metal insulator transition can be modified (and nearly disappear) in the film. NdNiO<sub>3</sub> is grown on (110) oriented single crystalline NdGaO<sub>3</sub> substrate, for three different thickness: specimen ( $a$ ) = 17 nm, specimen ( $b$ ) = 73 nm, specimen ( $c$ ) = 150 nm.

## 2 Experimental

Samples used in this experiment were deposited at 600 °C using RF sputtering process, followed by annealing in 170 bar O<sub>2</sub> for 48 hours in order to achieve the formation of stoichiometric NdNiO<sub>3</sub> [9]. The deposition time was varied in order to grow films of different thickness.

<sup>a</sup> e-mail: [patrick.laffez@univ-lemans.fr](mailto:patrick.laffez@univ-lemans.fr)

The conventional four probe technique was used to measure the resistance  $R$  as a function of temperature  $T$  in the range [4 K–320 K] using a PPMS quantum design probe. AFM measurements were carried out in air at room temperature using a Park Autoprobe CP Scanning Force Microscope which operates with an optical deflection sensor force. The AFM images were performed in contact mode with Si ultralever tips using a small repulsive force. X-ray diffraction was performed at room temperature after annealing, using an X-Pert Philips diffractometer using the Bragg-Brentano geometry, and  $\text{CuK}\alpha$  radiation. This configuration yield the out-of-plane parameter (i.e. perpendicular to the sample surface), and thus gives an indication of the epitaxial strain in the growth direction. Specimens for Transmission Electron Microscopy (TEM) and Electron Diffraction (ED) were prepared with two different orientations using mechanical polishing and ion milling. Samples were oriented along the [110] direction of the  $\text{NdGaO}_3$  substrate (planar view), or along the [001] direction (cross section). The TEM study was performed using a JEOL 4000EX microscope (with double tilt  $\pm 20^\circ$ ) operating at 400 keV (with a point resolution of 0.17 nm). High-resolution electron microscopy (HREM) images and selected area electron diffraction were used to study the microstructure. All HREM images were taken under the defocus condition close to the Scherzer defocus (around  $-550 \text{ \AA}$ ). Fourier transform (FT) and image processing was performed using the NIH Image 1.60/ppc software. The films thickness was measured by combining X-ray reflectivity and cross section TEM observations.

### 3 Results

In this section we present the electronic transport, X-ray diffraction analysis, high resolution electron microscopy and atomic force microscopy results, respectively.

#### 3.1 Electronic transport properties

The electrical measurements in Figure 1 clearly show a vanishing MI transition with decreasing sample thickness. MI transitions are clearly visible for sample (b) and sample (c), while the thinnest sample (a) exhibits a relatively temperature independent resistivity over the temperature range under investigation. When focusing on the range 120–130 K, a change in the sign of the slope  $\frac{d\rho}{dT}$  still appears indicating metallic behavior for sample (a). However this change is several orders of magnitude smaller than that of sample (b) and (c).

In the metallic state the temperature dependence of the resistivity, given in inset of Figure 1, also illustrates the significant difference between samples. According to the Drude approach and the Matthiessen rule, one can make use of the simplistic relation (1) to explain the temperature dependence as such:

$$\rho = \frac{m^*}{n(E_F) e^2 \tau} = \rho_d + \rho_L(T) \quad (1)$$

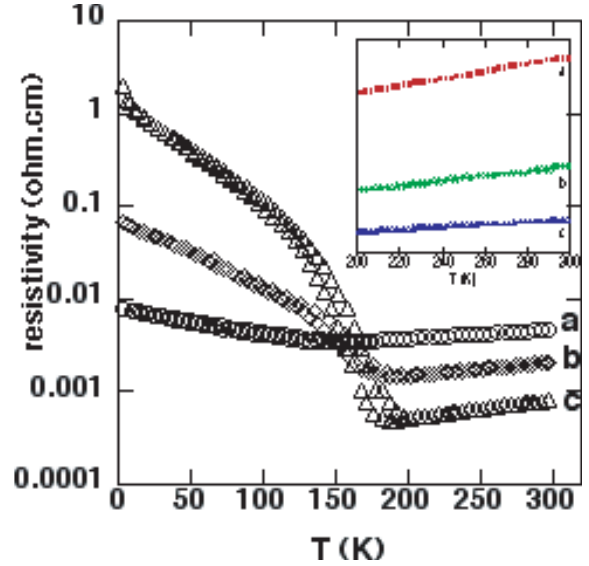


**Fig. 1.** Resistivity vs. temperature for  $\text{NdNiO}_3$  films of thickness (a) 17 nm, (b) 73 nm, (c) 150 nm. The corresponding transition temperatures are 129 K, 159 K, and 182 K, respectively. Inset shows the metallic conduction in the [200 K–300 K] range.

where  $m^*$  and  $n(E_f)$  are the electron effective mass and the number of electrons per volume at Fermi level respectively.  $1/\tau$  is the rate of electron scattering which takes many processes into account such as defects ( $\tau_d$ ) and phonons scattering ( $\tau_L$ ), and assumes the following relation:

$$\frac{1}{\tau} = \frac{1}{\tau_d} + \frac{1}{\tau_L} \quad (2)$$

$1/\tau_d$  is temperature independent while  $1/\tau_L$ , which is proportional to the number of phonons, increases with increasing temperature as such:

$$\frac{1}{\tau_L} \approx \frac{kT}{\Gamma} \quad (3)$$

$\Gamma$  is a parameter characterising the electron-lattice energy exchange.

Using the expressions above, the metallic quality can be defined as such (4):

$$Q = \frac{1}{\rho} \frac{d\rho}{dT} = \frac{k}{\frac{\Gamma}{\tau_d} + kT} \quad (4)$$

For a given temperature,  $Q$  only depends on the scattering processes and not on the electronic density of states at the Fermi level. At 280 K we found:  $Q(a) = 2.1 \times 10^{-3} \text{ K}^{-1}$ ,  $Q(b) = 2.9 \times 10^{-3} \text{ K}^{-1}$ ,  $Q(c) = 4 \times 10^{-3} \text{ K}^{-1}$ . For the bulk, a value of  $Q = 3.5 \times 10^{-3} \text{ K}^{-1}$  has been proposed in literature [10,11]. As expected, these results show more bulk-like behavior as the sample thickness increases. This suggests a different electron scattering process ( $\frac{\Gamma}{\tau_d}$ ) within the films. Naturally, we are not able to separate contributions from phonon and defects scattering; only a ratio is

available for discussion. However, note that the relative contribution from the defects scattering seems to be as smaller as the sample is thinner.

As shown in Figure 1, the metallic resistivity is one order of magnitude larger for sample (c) than for sample (a). Even if a difference between scattering times for each samples is reported, one can postulate that such an important difference might also come from the difference in electronic density of states in the vicinity of the Fermi level. In the ZSA approach [4], a possible sketch of the bare electronic band structure in the metallic state is shown in Figure 2. Such different O(2p)-Ni(3d) band overlaps could come from different Ni-O<sub>6</sub> octahedral distortions as supported by the following comments on the insulating state. In the insulating state, strong differences between activated regimes are indeed observed. According to the literature, no simple activation model, (such as the Arrhenius law), can be reasonably obtained from these results. Nevertheless, a qualitative description can be proposed. It appears that the thermal activation of the electrical resistivity increases with increasing thickness. Thermodynamically speaking, this would correspond to an increasing band gap with increasing thickness. Such results were confirmed thanks to a fitting procedure based on the Catalan et al. model [10], where two kinds of electrical transport have to be taken into account. In such a compound, the electrical transport occurs simultaneously through a classical activation type mechanism (first neighbor hopping), and a variable range hopping VRH (phonon-induced tunneling of electrons between localised states). A gap of 0.015 eV, 0.025 eV and 0.028 eV are estimated respectively for sample (a), (b) and (c). This result, according to the approach of Zaanen, Sawatzky and Allen [4] who describe the MIT by an opening and a closing of the O<sub>2p</sub>-Ni<sub>3d</sub> charge transfer gap from insulating to metallic state, would indicate that in the thinnest film (a), the gap is smallest. According to the ZSA approach, the change of the electronic band structure is related to the tilt of the O-Ni-O superexchange angle. Therefore, this result and that obtained in the metallic state indicate that the tilt angle mechanism, and its temperature dependence, is probably smaller and more frustrated as the thickness is reduced. This implies that the dynamics of the opening and closing of the gap is less efficient when the film is thin. As sketched in Figure 2, the thicker sample exhibits quite a large variation in its electronic band structure as a function of temperature, implying a high Fermi level density and the biggest gap, while the thermal variation of the electronic band structure in the smallest sample is almost inhibited. In this simple representation, we consider that the charge transfer constant ( $\Delta$ ) and the band width ( $W$ ) remain the same, which needs more justification, and is the subject of ongoing research.

### 3.2 X-ray diffraction analysis

Bulk NdNiO<sub>3</sub> crystallizes into an orthorhombic distortion of the perovskite: with space group Pbnm, with  $a = 5.389 \text{ \AA} \approx \sqrt{2}a_p$ ,  $b = 5.3816 \text{ \AA} \approx \sqrt{2}a_p$ , and

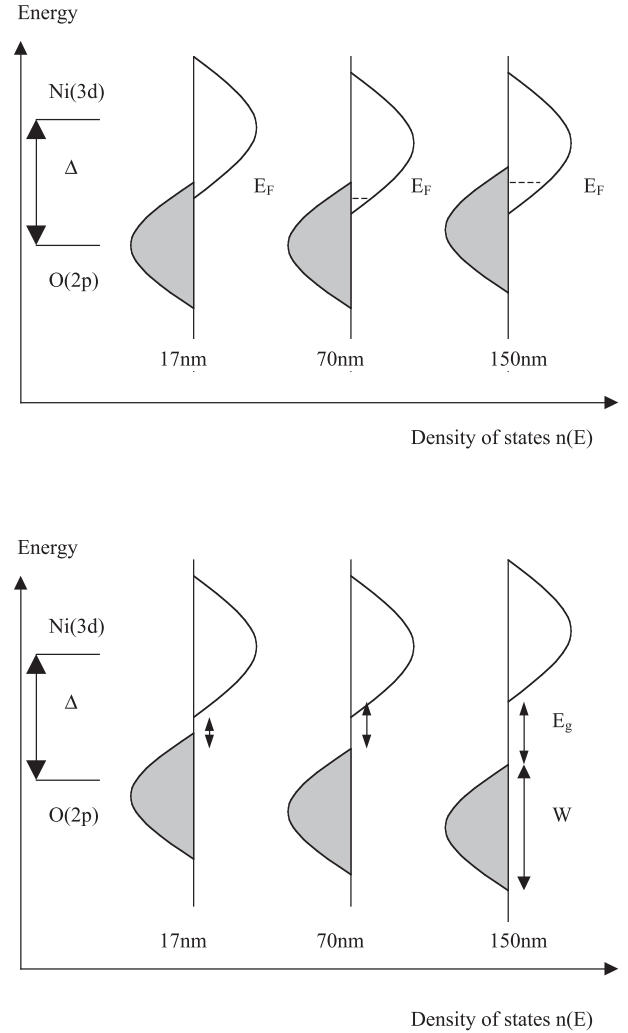


**Fig. 2.** Sketch of the temperature dependence of the electronic band structure of the three films.

$c = 7.61 \text{ \AA} \approx 2a_p$ . (Where  $a_p$  refers to the cubic perovskite cell parameter.) X-ray diffraction patterns of films grown on NdGaO<sub>3</sub> reveal that the growth orientation has a strong preference along the pseudo-cubic axis of the perovskite subcell. This is supported by the strong relative intensity of the ( $hh0$ ) and ( $00l$ ) peaks, compared with the ( $h00$ ) peak, which is usually the strongest peak in polycrystalline samples. No secondary phases are observed within the detection range of the X-ray diffraction. In Figure 3, an enlargement of the X-ray diagrams in the  $[101^\circ-115^\circ]$  range reveal a shift of the ( $008$ ) diffraction peak towards the higher angle which increasing film thickness. Using a cubic subcell we refined this parameter using the substrate reflections as an internal standard. In Figure 4, the out-of-plane pseudo-cubic parameter of the films decreases when the thickness increases, approaching the value of the bulk for the thickest film. Figure 4 also shows a plot of the variation of  $T_{MI}$  with respect to thickness. The relationship between film thickness and in-plane residual strain was reported in previous work where residual stress for such films was analyzed using the  $\sin^2 \psi$  method [12].

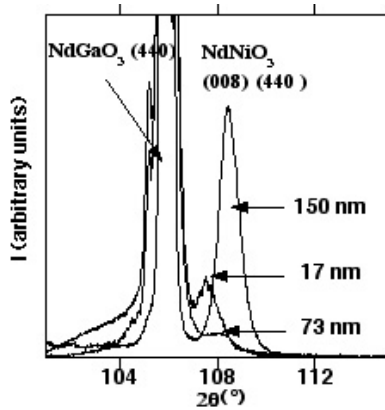


**Fig. 3.** X-ray diffraction patterns of NdNiO<sub>3</sub> films on NdGaO<sub>3</sub> for different thicknesses. The index refers to the Pbnm orthorhombic cell.

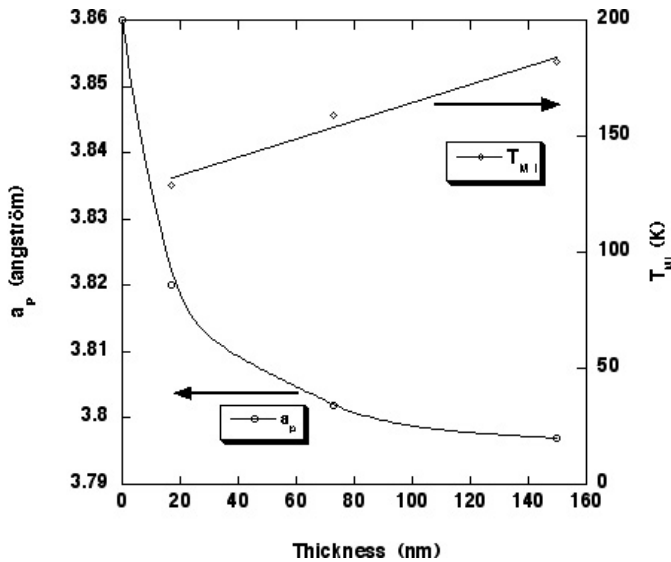


**Fig. 4.** Pseudo-cubic parameter in the growth direction and temperature of the MI transition versus thickness of the NdNiO<sub>3</sub> film. The cell parameter of the NdGaO<sub>3</sub> substrate is taken as the reference for a thin film thickness equal to zero.

Each film exhibits an in plane tensile stress whose magnitude depends on the sample thickness. We obtain a maximum tensile stress for the 150 nm thick film; the stress magnitude decreases with decreasing film thickness, and becomes negligible for the 17 nm thick film. Similar to the pressure-induced metallic phase stabilization reported by Obradors et al., we observed that the tensile stress tended to increase  $T_{MI}$ . A more detailed discussion dealing with the possible relationship between the metal-insulator transition temperature and residual stress can be found in reference [12]. These observations lead us to investigate the fine structure of the samples using HREM in order to understand why the less stressed materials (i.e. the thinnest) show an electrical behaviour that is very different to the usual ceramic.

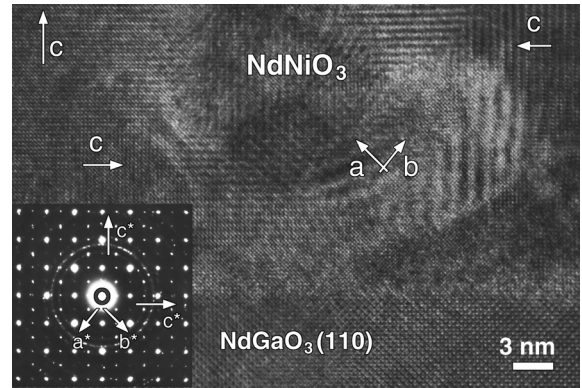


**Fig. 5.** Cross-section HREM micrograph pattern of the 73 nm thick NdNiO<sub>3</sub> film along the [001]<sup>\*</sup> zone axis. 90° oriented domains give the resultant diffraction pattern shown in the inset.

### 3.3 High resolution electron microscopy

Two samples of 17 nm and 73 nm thickness were examined by HREM. Figure 5 shows an HREM image of the 73 nm thick sample. ED and HREM patterns show that the film is hetero-epitaxially grown with twin related orientations of the domain structure. The grain boundaries are coherent with a simple crystallographic relationship. The ED pattern is the superposition of the substrate's diffraction pattern and of the film's different twinned domains. It can be indexed in the orthorhombic Pbnm (62) space group, with  $a = 5.389 \text{ \AA} \approx \sqrt{2}a_p$ ,  $b = 5.3816 \text{ \AA} \approx \sqrt{2}a_p$ , and  $c = 7.61 \text{ \AA} \approx 2a_p$  where  $a_p$  refers to the cubic perovskite cell. The corresponding limiting reflection conditions are  $0kl \ k = 2n$ ,  $h00 \ h = 2n$ ,  $0k0 \ k = 2n$ ,  $00l \ l = 2n$  and  $h0l \ h + l = 2n$ . Thicker films are supposed to show the same microstructure therefore, the physical properties should be close to those of the bulk sample. On the other hand, the HREM measurement shows a very different structure for the thinnest film (17 nm), as shown in the cross-sectional image (Fig. 6). One can observe a distinct contrast between the film and the substrate, even though NdGaO<sub>3</sub> and NdNiO<sub>3</sub> are theoretically isostructural with the same space group Pbnm. In the case of the substrate, the Fourier Transform (FT) pattern can be indexed with a Pbnm structure and [001]<sup>\*</sup> orientation. The FT of the film shows a pattern that is not compatible with this space group. While there is no extinction rule for  $(hk0)$  reflection in the Pbnm space group, the corresponding FT pattern of the film shows an  $h + k = 2n$  condition, suggesting a symmetry change. The corresponding HREM image shows perfect coherence of the lattice plane crossing the interface, suggesting an epitaxial growth of the film. However, lines of slightly brighter dots perpendicular to the substrate surface could be observed (Fig. 6). A plan-view HREM image, shown in Figure 7, suggests that these bright contrast lines are related to in-plane microtwin boundaries. The ED pattern of the planar view clearly combines the ED pattern of the substrate with that of the film. The extra spots in the ED shown in Figure 7 (white arrows) are a clear signature of the twin structure.

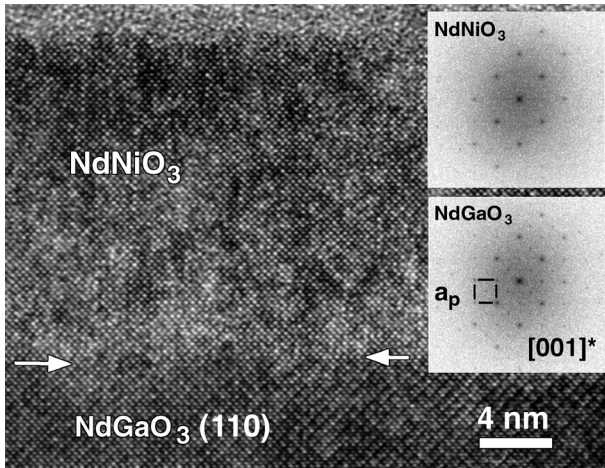


**Fig. 6.** Cross-section HREM micrograph of the 17 nm thick NdNiO<sub>3</sub> film along the [001]\* zone axis. Inset shows the optical diffraction pattern of the film and the substrate. The index refers to the Pbnm space group.

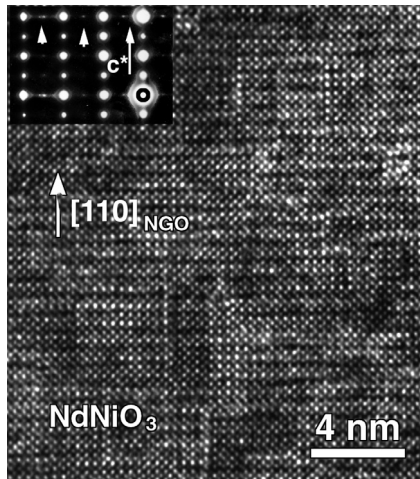


**Fig. 7.** Plane-view HREM micrograph and ED pattern of the 17 nm thick NdNiO<sub>3</sub> film along the [110]\* zone axis. White arrows show extra reflection and diffuse scattering related to the existence of oriented domains.

However, we also notice some diffuse streaking, which is also a signature of disorder in the [110] direction. The measurements show that for the thinnest film, the space group is no longer Pbnm. Despite minimal data collection due to the superposition of the ED pattern of the film and the substrate, it is reasonable to suggest that the space group is a maximal non-isomorphic subgroup of the Pbnm, with the extinction condition  $hk0, h+k=2n$ . For example, the Pna2<sub>1</sub> (33) should be consistent with the extinction rule:  $hk0, h+k=2n, 0kl, k=2n, h00, h=2n, 0k0, k=2n, 00l, l=2n$ . This suggestion is possible and further work is underway to determine the precise nature of the symmetry change and the exact space group.

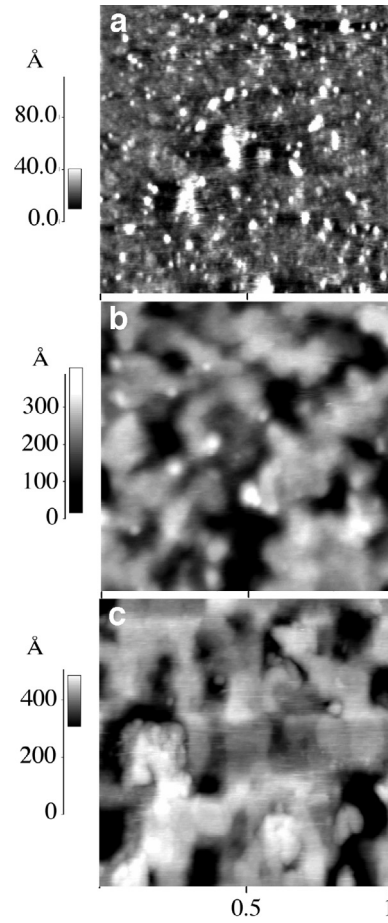


**Fig. 8.** AFM images of the surface of the NdNiO<sub>3</sub> films grown on (110)-NdGaO<sub>3</sub> substrates. The thickness of the films are (a) 17 nm, (b) 73 nm, (c) 150 nm. The scan size is 1 μm × 1 μm.

### 3.4 Atomic force microscopy

From the AFM images (Fig. 8), we can observe that the surface morphology and the surface roughness of the samples are quite different depending on the film thickness. Indeed, for the thinnest films (17 nm), the surface shows rounded grains with diameters in the range [250 Å–300 Å], large particles are also observed in certain parts of the films. These particles, whose size can reach 1500 Å, are shown to surround the small grains. The surface of the 73 nm thick films also appear to be constituted of grains. However, for such thicknesses, the mean diameter of the grains is shown to be higher (around 65 nm). In addition, the grains are shown to be more connected, leading to a well-organized surface morphology in the form of a “maze” with pores. For the thickest films (150 nm), we find that it becomes difficult to distinguish the grains from each other. This is probably due to their increasing size and their strong connectivity. The root mean square surface roughness ( $R_{rms}$ ) and the peak to valley surface roughness ( $R_{p-v}$ ) have been recorded over a 1 × 1 μm<sup>2</sup> square area. The average  $R_{rms}$  values are 9.21 Å, 65.7 Å, and 61.9 Å for the 17 nm, 73 nm, and 150 nm thick films respectively. The  $R_{p-v}$  values are 110 Å, 391 Å, and 507 Å

for the 17 nm, 73 nm, and 150 nm thick films respectively. As a result, we notice that the  $R_{rms}$  and  $R_{p-v}$  values increase with the thickness of the film (except for the  $R_{rms}$  values of the 73 nm and 150 nm thick films which are quite similar). This thickness dependence of the surface roughness characteristics has already been observed in others classes of materials such as  $\text{La}_{0.7}\text{Sr}_{0.3}\text{MnO}_3$  colossal magnetoresistive thin films. Such results have been explained in terms of large scale inhomogeneities which propagate upwards, thereby increasing the roughness of the film, or by considering an uphill Ehrlich-Schwoebel-type growth mechanism [13] which tends to increase the growth of hills compared to the valleys. This model seems to fit the present growth mechanism, however, it should be noted fact that it usually applies to as-grown films without the annealing process used in our samples.

## 4 Discussion and conclusion

In this study, we point out the influence of sample thickness on the thermal behavior of the resistance of  $\text{NdNiO}_3$  thin films and their micro-structural properties.

Firstly, it appears that the evolution of the transport properties may be partially related to the change in microstructure for the metallic state. Indeed, the scattering parameter ( $\frac{\Gamma}{\tau_d}$ ) of electrons in the metallic state tends to decrease when the microstructure (HREM) exhibits grains, and hence grain boundaries, which suggests that the defect scattering  $\tau_d$  may be relatively large compared with the phonon's ( $\Gamma$ ) as the thickness increases. In such an approach, it is reasonable to guess that the boundaries represent scattering centers for free electrons while for sample (a), a single domain observed by HREM (Fig. 6) would reduce such scattering. Even if the scattering processes are different, the large difference in conductivity observed in the metallic state might also come from differences in the density of states at the Fermi level ( $n(E_F)$ ). This is probably due to different electronic band structures. No spectroscopic studies to determine the density of empty and occupied levels in such films has been performed until now. We may, however, represent one possible mechanism. A qualitative representation, according to ZSA approach, is shown in Figure 2. In this representation, we suggest that the density of states at the Fermi level decreases with decreasing thickness.

In the insulating state, the charge transfer band gap  $E_g$  has been estimated and is found to decrease with decreasing thickness. According to the ZSA approach, this yield the electronic band structure sketched in Figure 2b. However it is far from obvious to deduce the value of the density of states as a function of energy.

In the framework of ZSA theory, the MIT is driven by the ability of the O-Ni-O angle to tilt with temperature. In this case, Ni-O-Ni angle frustration mechanism preventing thermal tilting of the angle could be invoked to explain the most important feature, which is the observation of the disappearance of Metal-Insulator transition for the thinnest sample (17 nm). Therefore the O-2p

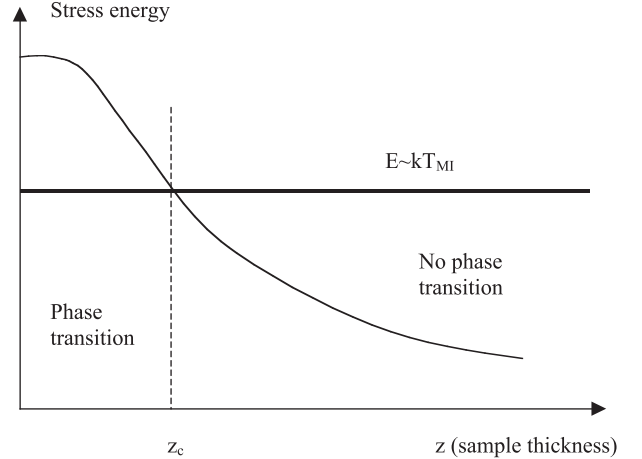


**Fig. 9.** Schematic representation of the stress energy versus thickness for thin films.

and Ni-3d band overlap would not change drastically as a function of temperature. However, this so-called frustration mechanism seems to be a more complex phenomena since HREM pictures (Fig. 6) reveal that the thinnest film ( $\sim 17$  nm) deposited on  $\text{NdGaO}_3$  does not exhibit the same structure as the two thicker films, but instead seems to adopt a deviation from the Pbnm orthorhombic space group. As a consequence, this new symmetry may be responsible of the quasi disappearance of the MI transition, and certainly affects the electronic band structure. Therefore ZSA approach does not seem sufficient. The reason why such symmetry breaking occurs in the thinnest samples is probably related to a modification of the epitaxial strain with thickness, as supported by the variation of the pseudo cubic lattice parameter of the film with decreasing thickness. Because there is a misfit, the thin film tries to accommodate its lattice parameter and then accumulate elastic energy. One can consider as a first approach the elastic energy gained through the shear stress as a driving parameter. If that shear stress energy reaches a critical value close to the characteristic value of the MIT, i.e. close to  $\sim kT_{MI}$ , one can expect a stress-induced phase transition. Depending on the sample thickness and the stress relaxation, the excess energy provided to the structure can extend over a finite distance. If that characteristic distance is close to the sample thickness a phase transition is then expected in the entire film. This phase transformation is sometimes observed in similar oxide systems where strains may stabilise new metastable phases [14]. In our case, we suggest that for thin films strain misfit induces a phase transition from Pnma to Pna2<sub>1</sub>, with some accommodation through microtwinning. For thicker films, twinned domains also appear without observing any phase transition. We summarize this in Figure 9. If we consider a misfit value of  $\Delta a \sim 0.06$  Å and a typical shear modulus of  $\sim 50$ – $100$  GPa, we get a rough approximation for the gained elastic energy at the interface of  $W \sim 1/2 \times G \times (\Delta a/a)^2 \times V \sim 3$ – $6$  meV, where  $V$  is the volume of the pseudo cubic cell. This value is to be

compared with  $kT_{MI} \sim 17$  meV. These two values scale approximately, which seems to support the influence of the elastic stress as a driving mechanism. This possible stress-induced phase transition may now explain why no residual stress was measured in our previous work [12]. The elastic energy may actually have been turned into cohesion energy of that new lattice. Of course, an improved description of the mechanical interaction must be proposed, and the new other point to be clarified is the value of the critical  $z_c$ . For this, a precise modeling of the mechanical energy relaxation through the thin film is required, but is not yet available. The interfacial defect nature has to be clarified as well.

We thank G. Niesseron for help during the film growth. We are grateful to Dr. N. Van Zandt (USA) for the revision of this manuscript. We would like to thank Dr. P. Lacorre and Dr. S. Kodjikan from Laboratoire des Fluorures, Université du Maine (France) for helpful discussions and support during the transport measurements. We are also grateful to L. Rossou (EMAT) for the TEM sample preparation. A part of this work was supported by the Tournesol program exchange France-Belgium 2003, by the CNRS “programme matériaux 2000–2001” (France), and by the framework of IUAP V-1, an initiative of the Belgian government.

## References

1. P. Lacorre, J.B. Torrance, J. Pannetier, A.I. Nazzal, P.W. Wang, T. Huang, J. Solid State Chem. **91**, 225 (1991)
2. J.F. DeNatale, P.H. Kobrin, Mater. Res. Soc. Symp. Proc. **479**, 145 (1997)
3. F. Capon, P. Laffez, J.-F. Bardeau, P. Simon, P. Lacorre, Appl. Phys. Lett. **81-4**, 619 (2002)
4. J. Zaanen, G.A. Sawatzky, J.W. Allen, Phys. Rev. Lett. **55**, 418 (1985)
5. J.B. Torrance, P. Lacorre, A.I. Nazzal, E.J. Ansaldo, Ch. Niedermayer, Phys. Rev. B **45**, 8209 (1992)
6. M. Zaghrioui, A. Bulou, P. Lacorre, P. Laffez, Phys. Rev. B **63**, 1534 (2001)
7. G. Frand, O. Bohnke, P. Lacorre, J.L. Fourquet, A. Carré, B. Eid, J.G. Théobald, A. Gire, J. Solid State Chem. **120**, 157 (1995)
8. X. Obradors, L.M. Paulius, M.B. Maple, J.B. Torrance, A.I. Nazzal, J. Fontcuberta, X. Granados, Phys. Rev. B **7**, 12353 (1993)
9. P. Laffez, R. Retoux, P. Boullay, M. Zaghrioui, P. Lacorre, G. Vantendeloo, Eur. Phys. J. Appl. Phys. **12**, 55 (2000)
10. G. Catalan, R.M. Bowman, J.M. Gregg, Phys. Rev. B **62**, 7892 (2000)
11. M.L. Medarde, J. Phys.-Cond. **9**, 1679 (1997)
12. P. Goudeau, P. Laffez, M. Zaghrioui, P.E. Elkaim, P. Ruello, Cryst. Eng. **5**, 317 (2002)
13. R. Desfeux, A. Da Costa, W. Prellier, Surf. Sci. **497**, 81 (2002)
14. See for ex. G. Van Tendeloo, O.I. Lebedev, S. Amelinckx, J. Magn. Magn. Mater. **211**, 73 (2000)